Thermal behavior of core-shell and three-shell layered clusters: Melting of Cu_1Au_{54} and $Cu_{12}Au_{43}$

Daojian Cheng, Shiping Huang, and Wenchuan Wang*
Division of Molecular and Materials Simulation, Key Lab for Nanomaterials, Ministry of Education, Beijing University of Chemical Technology, Beijing 100029, People's Republic of China
(Received 3 March 2006; revised manuscript received 7 July 2006; published 31 August 2006)

The meltinglike transition of the Cu_1Au_{54} and $Cu_{12}Au_{43}$ clusters is investigated by canonical Monte Carlo simulations, based on the second-moment approximation of the tight-binding potentials. The structures of both the Cu_1Au_{54} and $Cu_{12}Au_{43}$ clusters, shown to be icosahedral, are obtained from the so-called semi-grand-canonical ensemble Monte Carlo simulation at 100 K. A core-shell structure is found in Cu_1Au_{54}, with a single Cu atom in the center and 54 Au atoms on the surface and in interior shells of the cluster. On the other hand, $Cu_{12}Au_{43}$ possesses a three-shell onionlike structure, with a single Au atom located in the center, 12 Cu atoms in the middle shell, and 42 Au atoms occupying the surface shell of the cluster. Melting characteristics are observed by the changes in the caloric curve, heat capacity, root-mean-square bond-length fluctuation, and deformation parameter. It is found that doping of Au_{55} with a single Cu atom can sharply raise the melting point of the cluster. In addition, the three-shell onionlike structure can be transformed into the core-shell structure at the higher temperatures after melting. It is also found that surface segregation of Au atoms in Cu_1Au_{54} and $Cu_{12}Au_{43}$ occurs in the liquid phase. In addition, the simulation results show that the melting point increases with the concentration of Cu in the 55-atom Cu-Au bimetallic cluster.

DOI: 10.1103/PhysRevB.74.064117 PACS number(s): 61.46.Bc

I. INTRODUCTION

The melting of metal clusters has attracted considerable experimental and theoretical interest in recent years, due to their extensive applications in catalytic and optical fields.[1] An important observation for the metal clusters is that the melting temperature decreases with the reduction in the cluster diameter.[2] This thermodynamic description of cluster melting was validated for both free and supported iron clusters ranging from 150 to 10 000 atoms.[3] However, such a cluster size effect on melting is still in question. Experimental results by Haberland and co-workers[4–7] revealed that the melting temperatures of the sodium clusters with sizes ranging from 55 to 200 atoms are lower than the bulk sodium melting temperature, but are associated with large fluctuations, caused by the change of cluster size. Based on the *ab initio* simulations, Blundell and co-workers[8–10] also found that the melting points of sodium clusters present large size-dependent variations, which is in excellent agreement with the experiment. More interestingly, recent experimental results by Jarrold and co-workers showed that small tin clusters[11] and gallium clusters[12] could achieve a higher-than-bulk melting temperature. Also, Blundell and co-workers provided some theoretical explanations for the higher-than-bulk melting temperature in those clusters[13–16] very successfully by using the *ab initio* molecular dynamics simulation.

The thermal properties of bimetallic clusters are even more complex than that of the elemental ones. First, bimetallic clusters may display some specific properties,[17–19] compared with the elemental metal clusters. Second, their properties depend not only on size but also on composition and atomic ordering.[20] Some structural models were found in bimetallic clusters for their compositional ordering. For example, the core-shell structures were found in bimetallic clusters by experimental[21–24] and theoretical investigations,[25–41] which present unusual catalytic properties.[21,41] In addition, the three-shell onionlike structures (the *A-B-A* structure) were also predicted in bimetallic clusters by using theoretical methods,[37–41] in which the *A* atoms are enriched in the outer and third atomic shells, while the *B* atoms are enriched in the second atomic shell. Third, the introduction of impurities in an elemental metal cluster may shift its melting temperature, even by the substitution of a single impurity in the pure cluster with the size of more than a 100 atoms.[42]

Most of the investigations on bimetallic clusters were focused on the preparation and structural properties.[23,43] Only a few of the work was attempted to understand the meltinglike transition of bimetallic clusters.[44,45] Huang and Balbuena showed that the Cu-Ni bimetallic clusters exhibit a two-stage melting.[46] Sankaranarayanan *et al.* found that the meltinglike transition of both the free[47] and supported[48] Pd-Pt bimetallic clusters depends on the composition and size of clusters. Joshi and Kanhere[49,50] studied the finite-temperature behavior of Sn-doped Li clusters, and found that the impurity doped cluster Li_6Sn_1 possesses a lower melting temperature, compared with the host cluster Li_7. Aguado and co-workers[51,52] reported that the introduction of a single Li, Cs or K impurity in a pure sodium cluster can decrease the melting temperature. In contrast, Mottet *et al.*[42] found that the substitution of a single Ni or Cu impurity can increase the melting temperature of the icosahedral silver cluster. Also, thermal behavior of core-shell Li-Cs,[53] Na-Cs,[54] Ag-Co,[55] and Ag-Ni (Ref. 32) bimetallic clusters was studied theoretically. However, little attention has been paid to the more complex melting of three-shell onionlike bimetallic clusters.

The *ab initio* density-functional theory, based on the Kohn-Sham (KS) equations, has been successfully used to deduce the melting points of small tin,[13,14] gallium,[16] and

 ©2006 The American Physical Society

sodium clusters.[9] However, this method was proved to be difficult to simulate the thermal properties of large clusters, due to the computational expense of the KS approach.[9] In contrast, the lower computational expense of empirical potentials allows extensive searches for configurations. Previous investigations have showed that the empirical many-body potentials, such as the second-moment approximation of the tight-binding model,[56] can be applied to the melting of the pure[3,57–59] and alloy metal clusters.[32,42,55] In addition, the Monte Carlo (MC) method is faster in sampling the configuration space than molecular dynamics (MD),[20] and has been applied to the meltinglike transitions in single component metals[57,59–61] and bimetallic clusters.[44]

For the bulk material, the Cu-Au alloy can be used as a high-temperature structural material due to its excellent high-temperature strength properties.[62] Apart from the extensive studies on the Cu-Au bulk alloy,[62–64] there has been a steady growth of interest in Cu-Au bimetallic clusters both in experiment[65] and theory.[66–69] In the earlier papers, Kim *et al.*[65] prepared and characterized Cu-Au bimetallic clusters with the average size of 3.0 nm in chloroform. López *et al.*[66] simulated the 13-atom and 14-atom Cu-Au bimetallic clusters with different compositions by using the MD method, and found that the meltinglike transition of the mixed Cu-Au clusters is close to the meltinglike transition of Cu clusters. Van Hoof and Hou[67] studied the order-disorder phase transition and surface gold segregation phenomena of Cu_3Au bimetallic clusters by MC simulations. Johnston and coworkers investigated Cu-Au bimetallic clusters by using energy calculations[68] and genetic algorithm,[69] and showed that Au atoms lie on the surface and Cu atoms are located in the core. In our previous work[70] we investigated segregate phenomena in Cu-Au bimetallic clusters with decahedral structures, and the core-shell and three-shell onionlike structures were found in the 55-atom Cu-Au decahedral clusters.

The purpose of this work is to study the thermal behavior of 55-atom Cu-Au icosahedral clusters with the core-shell and three-shell onionlike structures by using canonical MC simulations. The different thermal properties between the pure and alloy clusters are discussed, and the effect of composition on the melting temperature of bimetallic clusters is addressed. In the next section, we present the computational methods. Section III describes our results and discussion, and Sec. IV offers our conclusions.

II. COMPUTATIONAL METHODS

A. Initial configurations setup

The initial atomic configurations of Cu-Au bimetallic clusters in this work were obtained by the semi-grand-canonical ensemble Monte Carlo (SEMI-GCMC) simulation at 100 K, based on the second-moment approximation of the tight-binding (TB-SMA) potentials. Simulations and our programming details for the initial configurations of the bimetallic clusters can be found elsewhere in the literature[67,71–73] and our previous work.[70] In our SEMI-GCMC simulation, the total number of atoms ($N=N_{Cu}+N_{Au}$), temperature (T) and chemical potential difference ($\Delta\mu=\mu_{Cu}-\mu_{Au}$) between the two species were fixed. N_{Cu} and N_{Au} were allowed to vary in our algorithm. The chemical composition at a given temperature was, therefore, obtained by performing the SEMI-GCMC simulation at a fixed value of the chemical potential difference $\Delta\mu$ between the two species in a cluster. For the bimetallic clusters, the SEMI-GCMC simulation method includes two types of trials in our program: (1) Displacement of each atom from its original position in a random direction, which corresponds to the relaxation and vibration movements and (2) random selection of the chemical type of an atom, corresponding to the fixed chemical potential difference $\Delta\mu$ between the two species and allowing the system to reach compositional equilibrium. The details of the simulation can also be referred to our previous work.[70]

B. The TB-SMA potential

In the Monte Carlo runs, we adopted the second-moment approximation of the TB-SMA model to describe the interaction between atoms. Within the TB-SMA potential,[56] the total energy of a system is expressed as

$$E_{total}=\sum_i (E_R^i+E_B^i), \tag{1}$$

where E_R^i and E_B^i are the Born-Mayer ion-ion repulsion and band terms, respectively. Both terms can be written for an atom i as

$$E_R^i=\sum_j Ae^{-p(r_{ij}/r_0-1)}, \tag{2}$$

$$E_B^i=-\left\{\sum_j \xi^2 e^{-2q(r_{ij}/r_0-1)}\right\}^{1/2}, \tag{3}$$

where A, ξ, p, q, and r_0 of the TB-SMA scheme are obtained by fitting to the experimental values of the cohesive energy, lattice parameters (by a constraint on the atomic volume), and independent elastic constants for the reference crystal structure at $T=0$ K. In addition, $r_0=a_0/\sqrt{2}$ (a_0 is the independent lattice constant for each pure system and for alloys), and r_{ij} is the distance between atoms i and j in the cluster.

For Cu-Au bimetallic clusters, the parameters are of different values for each of the different interactions (Cu-Cu, Au-Au, and Cu-Au). The potential models for pure elements (Cu-Cu and Au-Au) were derived by fitting to the pure metals and remained unchanged in the simulation. The Cu-Au potential parameters were obtained by fitting to the mechanical and thermodynamic properties of the bulk Cu_3Au. The potential parameters were developed by Cleri and Rosato,[56] which were employed for the theoretical study of Cu-Au bimetallic clusters with satisfactory results.[68,69] All the potential parameters used in this work are listed in Table I.

From the total cluster potential energy V_{clus} the average binding energy E_b for a N-atom cluster is defined as the positive quantity:

$$E_b=\frac{-V_{clus}}{N}. \tag{4}$$

TABLE I. Parameters of the TB-SMA potential for Cu-Au bimetallic clusters (Ref. 56).

	A (eV)	ξ (eV)	p	q	a_0 (Å)
Cu-Cu	0.0855	1.224	10.960	2.278	3.615
Au-Au	0.2061	1.790	10.229	4.036	4.079
Cu-Au	0.1539	1.5605	11.05	3.0475	3.615

C. Monte Carlo method

A canonical MC method was used to study the melting of Cu-Au bimetallic clusters. Temperature increased from 100 K in an increment of 50 K, but the increment was reduced to 10 K near the melting point. For each temperature, 1.1×10^6 MC steps were carried out for each atom. The first 1.0×10^5 steps/per atom were used to reach the equilibrium, where the fluctuation of total energy was less than 0.2%. The last 1.0×10^6 steps/per atom were used for the thermal average of various physical quantities. The equilibration configuration of the cluster after the MC steps at a given temperature was adopted as the starting configuration for the MC run at the higher temperatures.

To verify our program, we first simulated the melting temperature of Cu_{55}, which is about 780 K here. Obviously, the melting temperature of Cu_{55} (780 K) is in good agreement with the simulation result (776 K) from the MD method with the TB-SMA potential by Li *et al.*[74]

A number of indicators can be used to discuss the meltinglike transition in detail. In this work, apart from the caloric curve, the heat capacity C_v and the root-mean-square bond-length fluctuation δ were sampled to characterize the thermal behavior of clusters. The heat capacity C_v can be written as a function of the fluctuations in the potential energy:

$$C_v = \frac{(\langle E^2\rangle - \langle E\rangle^2)}{nk_BT}, \tag{5}$$

where E is the potential energy, n is the number of atoms in the cluster, k_B is the Boltzman constant, and T is the temperature.

The root-mean-square bond-length fluctuation δ is defined as

$$\delta = \frac{2}{n(n-1)}\sum_{i=1}^{n}\sum_{j=i+1}^{n}\frac{\sqrt{\langle r_{ij}^2\rangle_T - \langle r_{ij}\rangle_T^2}}{\langle r_{ij}\rangle_T}, \tag{6}$$

where n is the number of atoms in the cluster, r_{ij} is the distance between atoms i and j, and $\langle\ \rangle_T$ represents the ensemble average at temperature T.

To explore the shape change on melting, we define a deformation parameter ε_{def},[9,10] given by

$$\varepsilon_{def} = \frac{2Q_1}{Q_2+Q_3}, \tag{7}$$

where Q_1, Q_2, and Q_3 stand for the eigenvalues of the quadrupole tensor Q_{ij} with the descending order of $Q_1 \geqslant Q_2 \geqslant Q_3$. The quadrupole tensor Q_{ij} is defined as

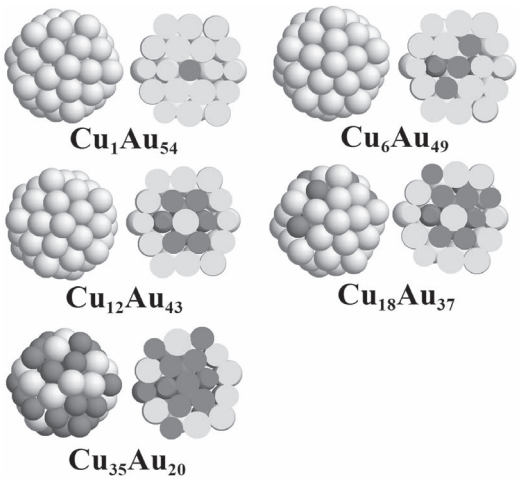

FIG. 1. The geometries of the ground state structures of Cu_1Au_{54}, Cu_6Au_{49}, $Cu_{12}Au_{43}$, $Cu_{18}Au_{37}$, and $Cu_{35}Au_{20}$ clusters at $T=100$ K. (black atoms, Cu; gray atoms, Au).

$$Q_{ij} = \sum_{I=1}^{N} R_{Ii}R_{Ij}, \tag{8}$$

where N is the total number of atoms in the cluster, and i and j run from 1 to 3. R_{Ii} and R_{Ij} are the ith and jth coordinates of atom I relative to the coordinate of the cluster center of mass, respectively. A value $\varepsilon_{def}=1$ is found for the spherical system ($Q_1=Q_2=Q_3$). Also, a value $\varepsilon_{def}>1$ represents a type of quadrupole deformation.

We define $g_{cm}(r)$ as the pair correlation function around the center of mass for the bimetallic clusters. $g_{cm}(r)$ is calculated from the trajectories of the MC simulation after equilibrium, given by

$$g_{cm}(r) = \frac{V}{N^2}\langle\sum_{i=1}^{n}\delta(\vec{r}_i - \vec{r}_{cm} - r)\rangle, \tag{9}$$

where N is the total atom number of the whole bimetallic cluster (55 in this work), V is the volume of the bimetallic cluster, n is the atom number counted, and $\vec{r}_{cm}$ is the coordinates of the center of mass at each MC step.

Here, we define $g^*_{cm}(r)=g_{cm}(r)/(V/N^2)$, and then the reduced pair correlation function $g^*_{cm}(r)$ is given by

$$g^*_{cm}(r) = \langle\sum_{i=1}^{n}\delta(\vec{r}_i - \vec{r}_{cm} - r)\rangle. \tag{10}$$

III. RESULTS AND DISCUSSION

A. Ground state structures

In this work, five typical 55-atom Cu-Au icosahedral clusters and two pure Cu_{55} and Au_{55} icosahedral clusters were studied. The lowest energy structures of the adopted clusters at 100 K were obtained by performing the SEMI-GCMC simulation. The lowest energy structures of Cu_{55} and Au_{55} are found to be two-shell Mackay icosahedron. Figure 1 shows the geometries of the ground state structures of the

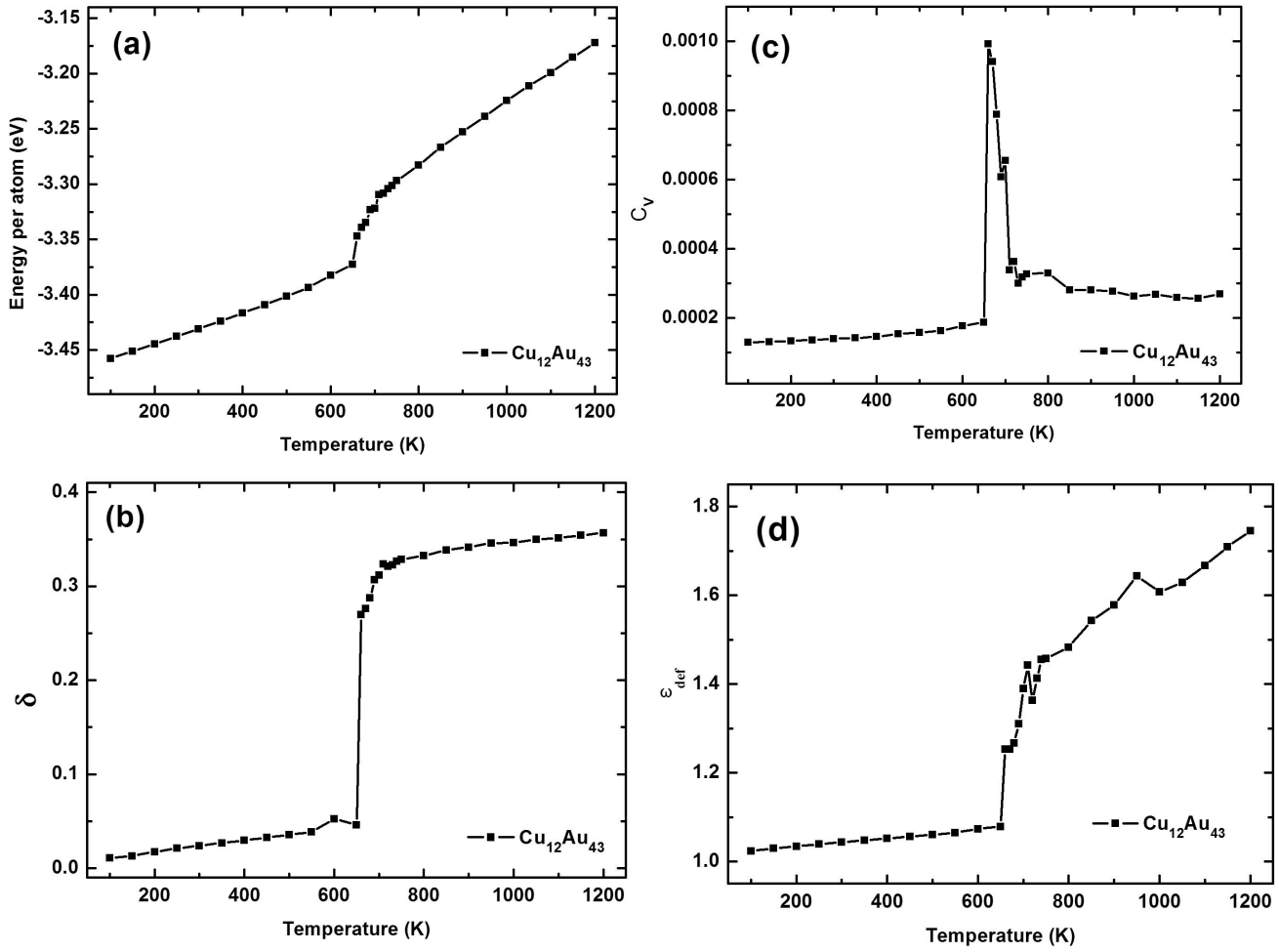

FIG. 2. Caloric curve, root-mean-square bond-length fluctuation, heat capacity, and deformation parameter of $Cu_{12}Au_{43}$: (a) the caloric curve, (b) the root-mean-square bond-length fluctuation δ, (c) the heat capacity C_v, and (d) the deformation parameter ε_{def}.

Cu_1Au_{54}, Cu_6Au_{49}, $Cu_{12}Au_{43}$, $Cu_{18}Au_{37}$, and $Cu_{35}Au_{20}$ clusters at 100 K. The lowest energy geometry of Cu_1Au_{54} is of an icosahedral core-shell structure, where a single Cu atom occupies the center of the cluster and the remaining 54 Au atoms form two spherical shells around it. This structure is in good agreement with the results from the genetic algorithm[69] and energy calculation.[68] We also found that the Cu_6Au_{49} and $Cu_{35}Au_{20}$ clusters achieve an icosahedral core-shell structure with an Au-enriched surface and a Cu-enriched core. In addition, the $Cu_{12}Au_{43}$ cluster is found to be an icosahedron with the three-shell onionlike structure. In this structure, a single Au atom occupies the central site, and 12 Cu atoms are in the middle shell, covering the central single Au atom completely, while the remaining 42 Au atoms lie in the surface shell to form the Au-Cu-Au structure. It is also found here that the $Cu_{18}Au_{37}$ cluster possesses an icosahedral three-shell onionlike structure, where the Au atoms are enriched on the surface, and the Cu atoms are in the middle shell, while a single Au atom is located in the center.

B. Meltinglike transition in $Cu_{12}Au_{43}$

Figure 2(a) shows the temperature dependence of the average total energy per atom of $Cu_{12}Au_{43}$, which represents the caloric curve of the cluster. It is found in Fig. 2(a) that the average total energy per atom for the $Cu_{12}Au_{43}$ cluster increases monotonically with temperature in the early stage. Then, a distinguishable sudden increase in the caloric curve occurs, corresponding to the melting transition of the cluster. However, similar behavior could also be found in a solid-solid or solid-glass phase transition. To confirm the occurrence of a solid-liquid transition, the root-mean-square bond-length fluctuation δ as a function of temperature was calculated, as shown in Fig. 2(b). At low temperatures the root-mean-square bond-length fluctuation δ is small. As the temperature reaches 660 K, the value of δ is of a giant jump from 0.05 to 0.3, due to the emergence of the liquid phase, and finally keeps stable at about 0.3. To identify the melting temperature, the heat capacity C_v is plotted in Fig. 2(c). Consistent with the literature,[9,47,54] the melting point is defined as the temperature with the maximum of the peak in the heat capacity C_v. For the $Cu_{12}Au_{43}$ cluster, the sharp peak with its maximum height at about 660 K in the heat capacity C_v corresponds to the distinguishable sudden increase in the caloric curve and the giant jump in the root-mean-square bond-length fluctuation δ. Therefore, we estimate that the melting temperature of $Cu_{12}Au_{43}$ is about 660 K.

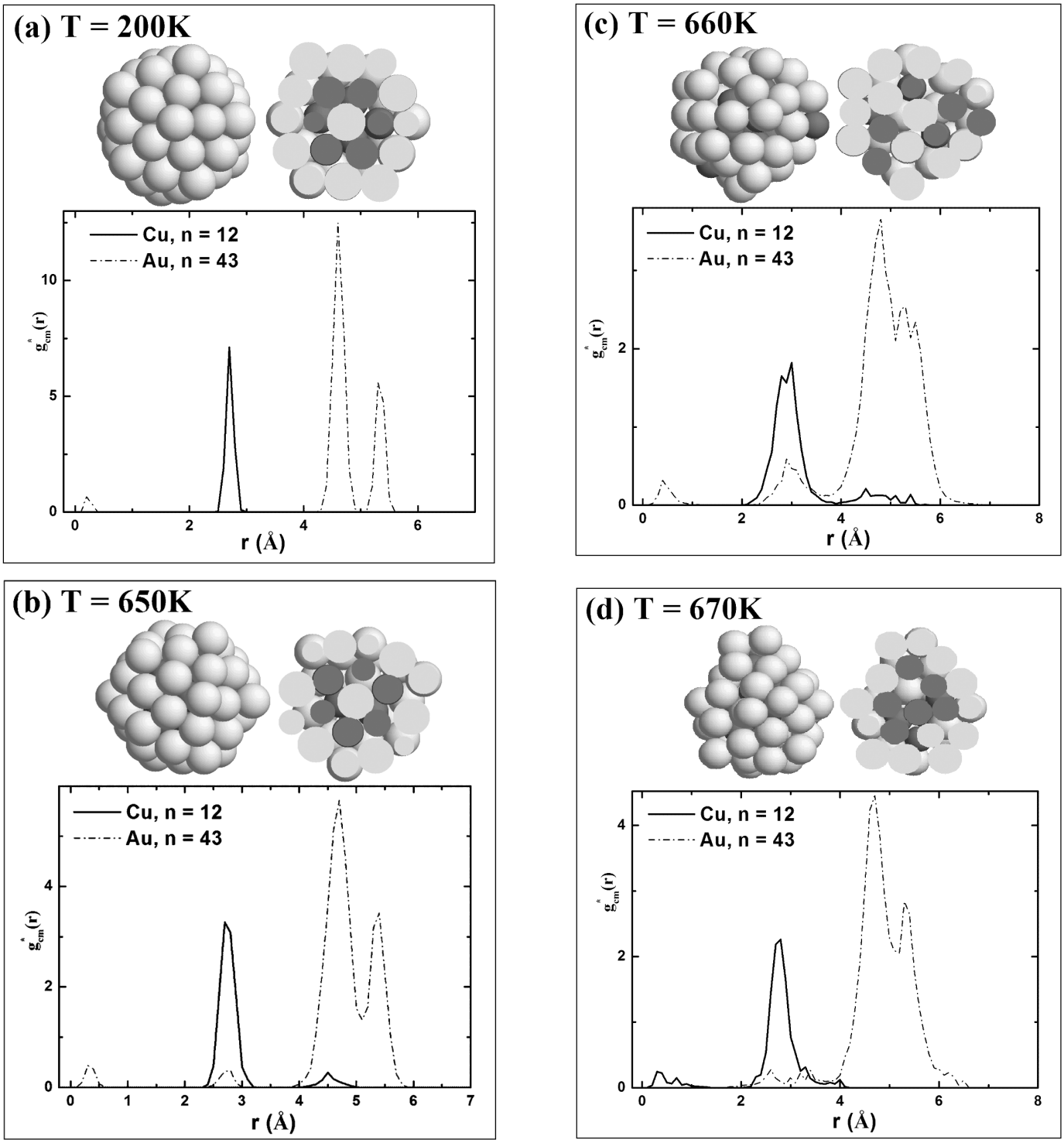

FIG. 3. The snapshots (black atoms, Cu; gray atoms, Au) and reduced pair correlation functions (Cu, solid line, $n=12$; Au, short dash-dotted line, $n=43$) of $Cu_{12}Au_{43}$ at (a) 200 K, (b) 650 K, (c) 660 K, and (d) 670 K.

The shape of $Cu_{12}Au_{43}$ before and after melting was monitored by the variation of the deformation parameter ε_{def} from Eq. (7). Figure 2(d) shows the temperature dependence of the deformation parameter ε_{def} of the $Cu_{12}Au_{43}$ cluster. At the lower temperatures before melting, the deformation parameter ε_{def} remains almost unchanged with the value of about 1, indicating that the $Cu_{12}Au_{43}$ cluster keeps the compact icosahedral structure before cluster melting. After the cluster melting, the system shows a quadrupole deformation with $\varepsilon_{def} \approx 1.6$, indicating that the $Cu_{12}Au_{43}$ cluster changes from a spherical shape to a somewhat oval shape upon melting. A similar phenomenon was observed earlier by Chacko *et al.*[9] for the Na_{55} cluster. This change may be due to the fact that the cluster undergoes a spontaneous shape deforma-

tion to lower its free energy in the liquid phase.[9]

The melting process of the $Cu_{12}Au_{43}$ cluster can be further explored by the snapshots and reduced pair correlation functions of the cluster at the temperatures before and after melting. Figure 3 shows the snapshots and reduced pair correlation functions of $Cu_{12}Au_{43}$ at 200, 650, 660, and 670 K, respectively. At the lower temperatures, e.g., $T=200$ K, the cluster retains the compact icosahedral structure. This is clearly seen in the snapshots and reduced pair correlation function $g(r)$ plotted in Fig. 3(a). The reduced pair correlation function $g(r)$ shows four peaks, corresponding to the four different coordination shells: the subshell of surface shell with the atoms in vertex positions, the subshell of surface shell with the atoms in nonvertex positions, the inner shell, and the central atom. Moreover, the coordination shells of Cu and Au atoms are clearly distinguished, and the three-shell onionlike structure still remains at 200 K with the 12 Cu atoms occupying the inner shell [see Fig. 3(a)].

With the temperature increasing, the peaks in the reduced pair correlation function become broader and lower, and some peaks even disappear. At a higher temperature of 650 K before melting, some mixing is found in the two subshells of surface shell [see Fig. 3(b)]. This involves the movement of atoms on the cluster surface. Particularly, the mixing of the coordination shells of Cu and Au occurs, although it is weak. By observing the snapshots and reduced pair correlation function $g(r)$ [see Fig. 3(b)], we can see that the $Cu_{12}Au_{43}$ cluster still maintains the three-shell onionlike structure at 650 K.

Finally, the melting transition from the solid to liquid phase of $Cu_{12}Au_{43}$ occurs at 660 K. The reduced pair correlation function $g(r)$ of $Cu_{12}Au_{43}$ shows that the two peaks, corresponding to the two subshells of the surface shell, merge into one peak at 660 K [see Fig. 3(c)]. The peak in the heat capacity at the melting temperature of 660 K is associated with the merging of the two subshells of the $Cu_{12}Au_{43}$ cluster. Also, the substantial mixing of Cu and Au atoms is observed.

At the higher temperatures after melting, $T=670$ K, the $Cu_{12}Au_{43}$ cluster is completely in a liquid phase [see Fig. 3(d)]. Interestingly, all the Cu atoms lie in the core, covered by the Au atoms, forming the core-shell structure, and the center Au atom is replaced by a Cu atom after the melting of the cluster at 670 K. It seems that the three-shell onionlike structure can be transformed into the core-shell structure at the higher temperatures after melting, which is consistent with the result that the three-shell onionlike structure could be metastable, reported by Baletto *et al.*[39]

It is also interesting to describe the melting process by plotting the histograms of the potential energy, which gives the distribution of the potential energy. Figure 4 shows the histograms of the potential energy for $Cu_{12}Au_{43}$ at 650 K (below the melting point) and 660 K (melting point). It is found in Fig. 4(a) that the potential energy density gives a peak at 650 K (below the melting point), indicating that the system is in the solid phase. However, at the melting temperature of 660 K, the histogram becomes broader, and the potential energy density is split into two peaks, as shown in Fig. 4(b). This behavior is due to the appearance of the liquid phase at 660 K. Consequently, the position of the new peak in the histogram of the potential energy corresponds to the energy of the liquid phase at 660 K.

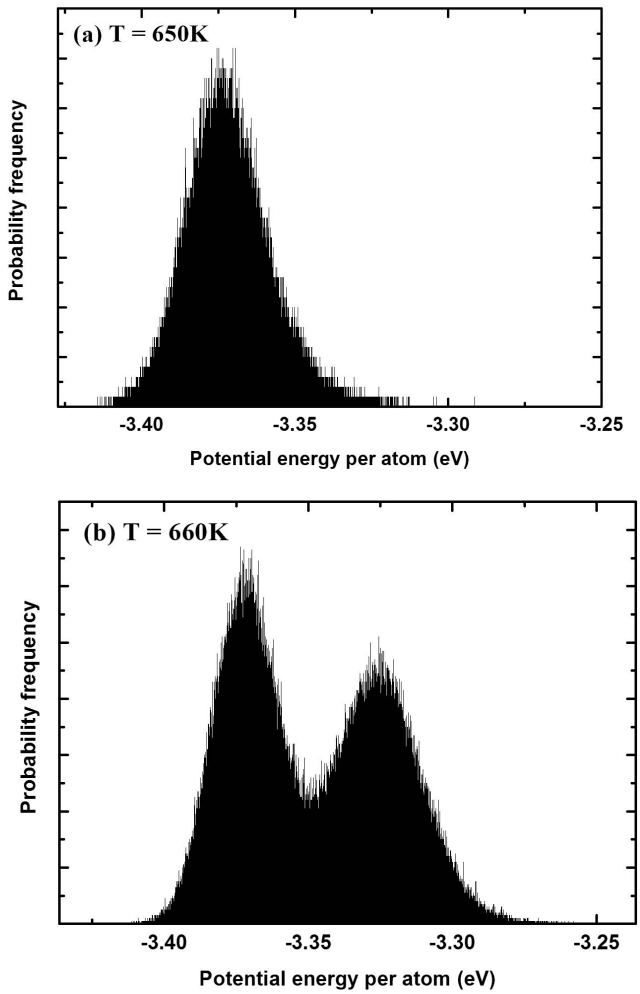

FIG. 4. Distribution of the potential energy for $Cu_{12}Au_{43}$ at (a) 650 K (below the melting point); (b) 660 K (melting point). Averages over 100 steps in the MC simulation are collected in the histogram.

C. Meltinglike transition in Cu_1Au_{54}

Figures 5(a)–5(c) show the caloric curve, the temperature dependence of the root-mean-square bond-length fluctuation δ, and the heat capacity C_v of Cu_1Au_{54}. The indicators employed here are exactly the same as those for the $Cu_{12}Au_{43}$ cluster. As is seen from Fig. 5(a), the distinguishable sudden increase in the caloric curve implies the occurrence of the melting transition of the cluster. The giant jump in the curve of the root-mean-square bond-length fluctuation, δ, changing with the temperature, indicates the appearance of the liquid phase [see Fig. 5(b)]. Moreover, the heat capacity C_v of Cu_1Au_{54} shows a sharp peak with its maximum height at about 530 K, corresponding to the distinguishable sudden increase in the caloric curve and the giant jump in the root-mean-square bond-length fluctuation δ of Cu_1Au_{54} [see Fig. 5(c)]. Thus, we estimate that the melting temperature of Cu_1Au_{54} is about 530 K.

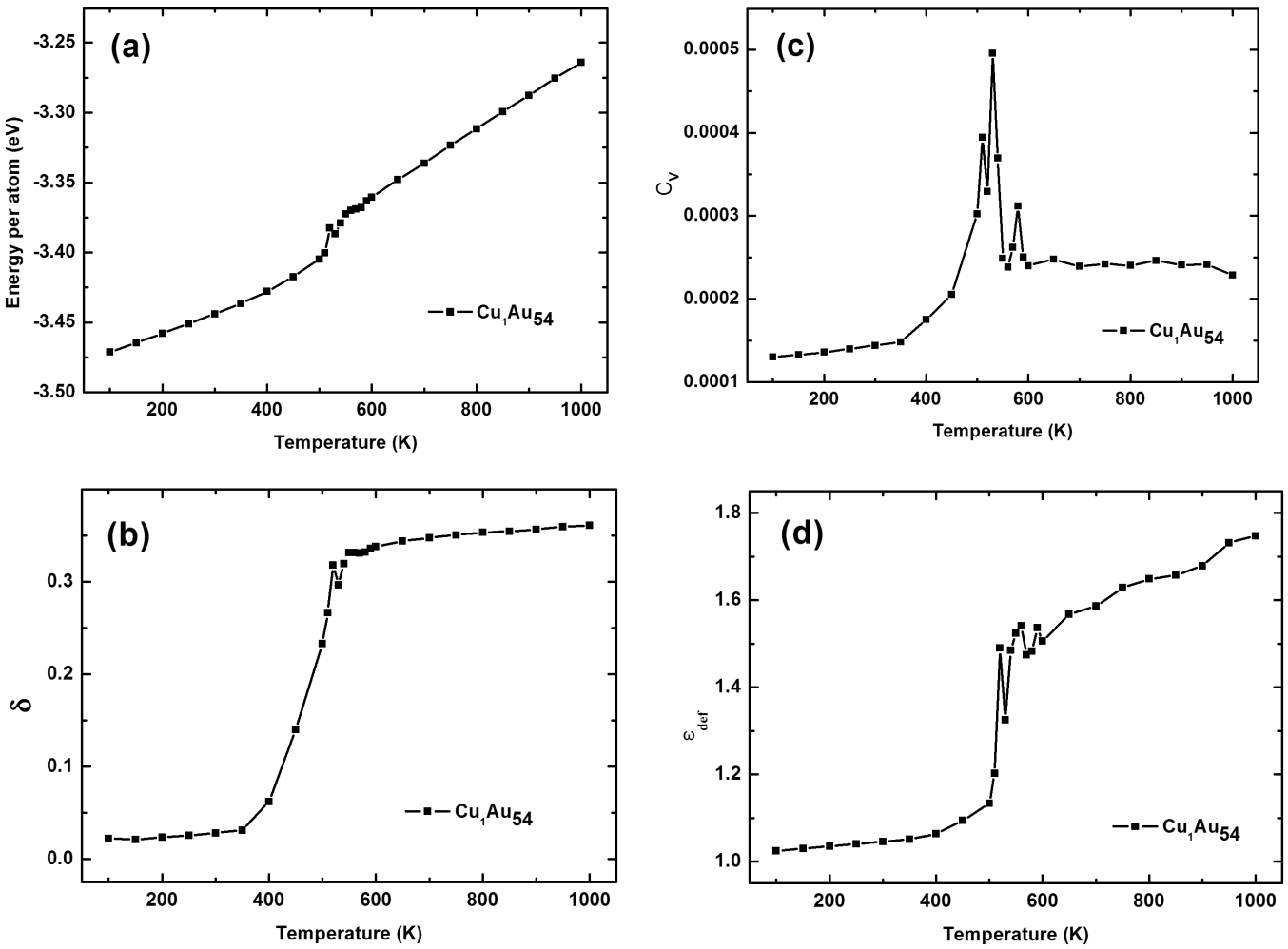

FIG. 5. Caloric curve, root-mean-square bond-length fluctuation, heat capacity, and deformation parameter of Cu_1Au_{54}: (a) the caloric curve, (b) the root-mean-square bond-length fluctuation δ, (c) the heat capacity C_v, and (d) the deformation parameter ε_{def}.

In Fig. 5(d), we show the temperature dependence of the deformation parameter ε_{def} of Cu_1Au_{54}. The deformation behavior is similar to that of the $Cu_{12}Au_{43}$ cluster. At the lower temperatures before melting, it is found that $\varepsilon_{def} \approx 1$, corresponding to the stable 55-atom Mackay icosahedral ground state. At the higher temperatures after cluster melting, a quadrupole deformation is found for the Cu_1Au_{54} cluster with $\varepsilon_{def} \approx 1.6$, corresponding to the shape changes from a spherical shape to a somewhat oval shape after melting.

Figure 6 shows the snapshots and reduced pair correlation functions of Cu_1Au_{54} at 200, 510, 530, and 550 K. At 200 K, when the cluster is still solid, there is a clear separation in the four different coordination shells formed by Cu and Au atoms [see Fig. 6(a)], indicating that the initial 55-atom Mackay icosahedral ground state structure is completely preserved. At the temperature of 510 K near melting, there is some mixing in the two subshells of a surface shell, corresponding to the atomic motion on the surface shell upon heating [see Fig. 6(b)]. This behavior results in the emergence of a small additional peak in the heat capacity C_v of Cu_1Au_{54} at 510 K [see Fig. 5(c)].

At the melting point 530 K, the sharp peaks in the pair correlation function $g(r)$ disappear [see Fig. 6(c)], which indicates that the cluster is not structured anymore upon melting. The single Cu atom moves away from the central site, but the core-shell structure still remains with the single Cu atom lying in the inner shell of the cluster. At higher temperatures after melting, $T=550$ K, the whole cluster is liquidlike [see Fig. 6(d)], but the single Cu atom still stays in the core of the cluster. It means that surface segregation of Au atoms still remains in the liquid state for the Cu_1Au_{54} cluster.

D. Effect of composition on melting

The melting behaviors were investigated for different compositions of the 55-atom Cu-Au bimetallic cluster, namely, 0%, 2%, 11%, 22%, 33%, 64%, and 100% Cu, corresponding to the structures of Au_{55}, Cu_1Au_{54}, Cu_6Au_{49}, $Cu_{12}Au_{43}$, $Cu_{18}Au_{37}$, $Cu_{35}Au_{20}$, and Cu_{55}. We employed the same indicators as those for the $Cu_{12}Au_{43}$ and Cu_1Au_{54} clusters to identify the melting temperatures for Au_{55}, Cu_6Au_{49}, $Cu_{18}Au_{37}$, $Cu_{35}Au_{20}$, and Cu_{55}. For the limit of the paper length, we will not discuss it in detail. To verify the occurrence of the melting transition, we gave the caloric curves of the Au_{55}, Cu_1Au_{54}, Cu_6Au_{49}, $Cu_{12}Au_{43}$, $Cu_{18}Au_{37}$, $Cu_{35}Au_{20}$,

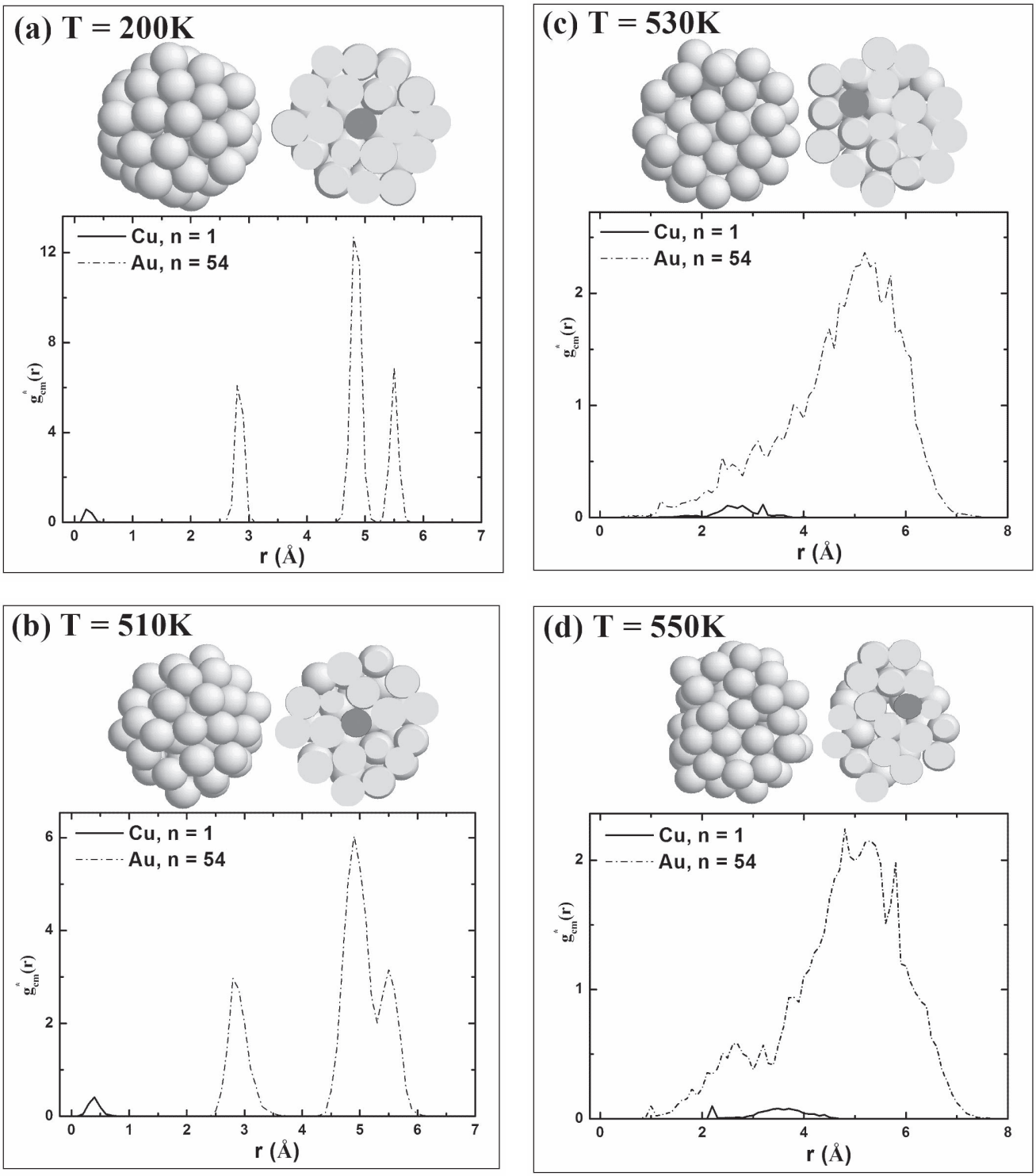

FIG. 6. The snapshots (black atoms, Cu; gray atoms, Au) and reduced pair correlation functions (Cu, solid line, $n=1$; Au, short dash-dotted line, $n=54$) of Cu_1Au_{54} at (a) 200 K, (b) 510 K, (c) 530 K, and (d) 550 K.

and Cu_{55} cluster, as shown in Fig. 7. Apparently, distinguishable sudden increases in the caloric curves of those clusters correspond to the melting transition of the clusters.

Figure 8 shows the melting point changing with the concentration of Cu in the 55-atom Cu-Au bimetallic cluster. It is found in Fig. 8 that there is a monotonous increase in the melting temperature with the concentration of Cu in the 55-atom Cu-Au bimetallic cluster. Also, for the low Cu-concentration the rise in the melting temperature, with respect to a lower Cu concentration, is quite high as against that seen for higher Cu concentration. This behavior means that a very small amount of Cu is sufficient to raise the melting temperature of Au clusters substantially. The melting points for the different concentrations of Cu in the 55-atom

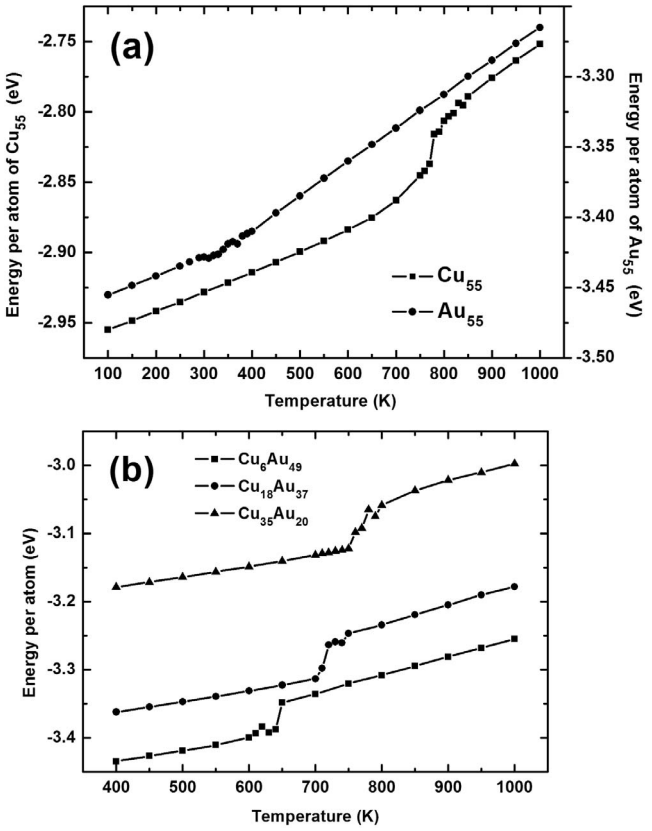

FIG. 7. Caloric curves of Au_{55}, Cu_6Au_{49}, $Cu_{18}Au_{37}$, $Cu_{35}Au_{20}$, and Cu_{55}. (a) Au_{55} and Cu_{55}. (b) Cu_6Au_{49}, $Cu_{18}Au_{37}$, and $Cu_{35}Au_{20}$.

Cu-Au bimetallic clusters are also listed in Table II.

The reason for the melting point changing with the concentration of Cu in the 55-atom Cu-Au cluster may be due to the relative stability of those clusters. We monitored it by calculating the average binding energy E_b of those clusters from Eq. (4). The average binding energy E_b, which is the positive quantity of the total potential energy divided by the total number of atoms (N=55 in this work), indicates the relative stability of clusters with different compositions. For the 55-atom Cu-Au clusters here, the global-minimum energies used to calculate the average binding energy were obtained by using the SEMI-GCMC simulation at 100 K. Figure 8 shows the composition dependence of the average binding energy. In those 55-atom Cu-Au clusters, there is also a monotonous increase in the average binding energy, which is similar to the tendency of the melting point changing with the concentration of Cu in the 55-atom Cu-Au bimetallic clusters (see Fig. 8). This observation agrees with the rule that the stabler the cluster, the higher the melting point.

It is interesting to find that the melting temperature of Au_{55} (380 K) is much lower than that of Cu_1Au_{54} (530 K),

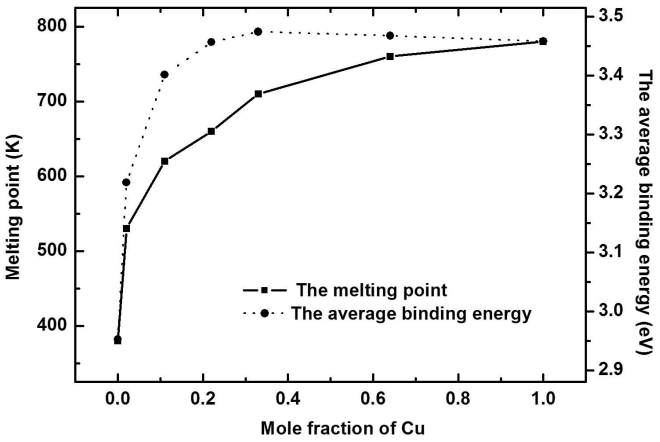

FIG. 8. The melting point and average binding energy changing with the concentration of Cu in the 55-atom Cu-Au bimetallic cluster.

although the Cu_1Au_{54} cluster comes from the substitution of a single Cu impurity in the Au_{55} cluster. This behavior may be due to the sharp increase in the average binding energies of Au_{55} and Cu_1Au_{54} (see Fig. 8). To further explore the reason for the pronounced increase of the melting point observed after doping a single Cu atom, we calculated the impurity solution energy, ΔE_{imp}, of one impurity Cu atom in the Au clusters of N atoms as follows:[42]

$$\Delta E_{imp} = E(\mathrm{Au}_{N-1}\mathrm{Cu}) - E(\mathrm{Au}_N) + \frac{1}{N}[E(\mathrm{Au}_N) - E(\mathrm{Cu}_N)], \tag{11}$$

where $E(\mathrm{Au}_{N-1}\mathrm{Cu})$, $E(\mathrm{Au}_N)$, and $E(\mathrm{Cu}_N)$ are the total energies of the mixed and pure clusters, with N=55 in this work. The negative sign in the impurity solution energy means that the state can be accessed favorably in terms of substituting the Au atom with a different one in the Au clusters. Here, we calculated the impurity solution energy of Cu_1Au_{54} by substituting the central Au atom with a Cu atom at 100 K. The value of ΔE_{imp} is −1.385 eV. It means that the substitution of the Cu atom in the 55-atom Au clusters can be accessed favorably, and can thus increase the melting temperature of the 55-atom icosahedral Au cluster.

In a previous work, as indicated in the Introduction, Joshi and Kanhere[50] found that doping the single Sn impurity can decrease the melting temperature of the host cluster Li_7. Aguado and co-workers[51,52] found that the substitution of a single Li, Cs, or K impurity can also decrease the melting temperature of the 55-atom icosahedral sodium cluster. In contrast, Mottet *et al.*[42] found that the introduction of a single Ni or Cu impurity in icosahedral silver clusters causes an increase of the melting temperature. In our work, the

TABLE II. Variation of the melting point with a composition for 55-atom Cu-Au bimetallic clusters in this work.

Composition	Au_{55}	Cu_1Au_{54}	Cu_6Au_{49}	$Cu_{12}Au_{43}$	$Cu_{18}Au_{37}$	$Cu_{35}Au_{20}$	Cu_{55}
Melting point (K)	380 K	530 K	620 K	660 K	710 K	760 K	780 K

melting behavior of icosahedral Cu_1Au_{54} is similar to that of icosahedral $Ag_{54}Ni_1$ and $Ag_{54}Cu_1$,[42] and is different from that of icosahedral Li_7Sn_1, $Na_{54}Li_1$, $Na_{54}Cs_1$, and $Na_{54}K_1$.[50–52] This may be explained by the fact that Au and Ag are much more stiff than Na and Li.[42,75]

IV. CONCLUSIONS

In this work, we have investigated the thermal characteristics of Cu_1Au_{54} with the core-shell structure and $Cu_{12}Au_{43}$ with the three-shell onionlike structure through MC method, using the TB-SMA potentials. The melting of the clusters is mainly detected by the change of the heat capacity C_v. The results indicate that the melting temperature of Au_{55} (380 K) is much lower than that of Cu_1Au_{54} (530 K), which means that doping Au_{55} with an impurity Cu atom can modify the meltinglike transition of Au_{55}. On the other hand, $Cu_{12}Au_{43}$ exhibits the core-shell structure after melting, indicating that the three-shell onionlike structure can be transformed into the core-shell structure at the higher temperatures after melting. Moreover, Au atoms in $Cu_{12}Au_{43}$ still lie on the surface, and the single Cu atom in Cu_1Au_{54} is still located in the core even in the liquid phase. The melting point increases with the concentration of Cu atoms in the 55-atom Cu-Au bimetallic cluster, due to the relative stability of those clusters, as is shown in Fig. 8. The simulation results suggest that it is possible to change the melting point of the pure cluster by doping some impurities.

ACKNOWLEDGMENTS

This work was supported by the National Natural Science Foundation of China (Grants No. 20476004 and No. 20236010), and the National Basic Research Program of China (Grant No. G2003CB615807).

*To whom correspondence should be addressed: Fax: +86-10-64427616; Email address: wangwc@mail.buct.edu.cn

[1] R. L. Johnston, *Atomic and Molecular Clusters* (Taylor and Francis, London, 2002).
[2] J. P. Borel, Surf. Sci. **106**, 1 (1981).
[3] F. Ding, A. Rosen, S. Curtarolo, and K. Bolton, Appl. Phys. Lett. **88**, 133110 (2006).
[4] M. Schmidt, R. Kusche, W. Kronmuller, B. von Issendorff, and H. Haberland, Phys. Rev. Lett. **79**, 99 (1997).
[5] M. Schmidt, R. Kusche, B. von Issendorff, and H. Haberland, Nature (London) **393**, 238 (1998).
[6] R. Kusche, T. Hippler, M. Schmidt, B. von Issendorff, and H. Haberland, Eur. Phys. J. D **9**, 1 (1999).
[7] H. Haberland, T. Hippler, J. Donges, O. Kostko, M. Schmidt, and B. von Issendorff, Phys. Rev. Lett. **94**, 035701 (2005).
[8] P. Blaise and S. A. Blundell, Phys. Rev. B **63**, 235409 (2001).
[9] S. Chacko, D. G. Kanhere, and S. A. Blundell, Phys. Rev. B **71**, 155407 (2005).
[10] M.-S. Lee, S. Chacko, and D. G. Kanhere, J. Chem. Phys. **123**, 164310 (2005).
[11] A. A. Shvartsburg and M. F. Jarrold, Phys. Rev. Lett. **85**, 2530 (2000).
[12] G. A. Breaux, R. C. Benirschke, T. Sugai, B. S. Kinnear, and M. F. Jarrold, Phys. Rev. Lett. **91**, 215508 (2003).
[13] K. Joshi, D. G. Kanhere, and S. A. Blundell, Phys. Rev. B **66**, 155329 (2002).
[14] K. Joshi, D. G. Kanhere, and S. A. Blundell, Phys. Rev. B **67**, 235413 (2003).
[15] S. Krishnamurty, K. Joshi, D. G. Kanhere, and S. A. Blundell, Phys. Rev. B **73**, 045419 (2006).
[16] S. Chacko, K. Joshi, and D. G. Kanhere, Phys. Rev. Lett. **92**, 135506 (2004).
[17] J. H. Sinfelt, *Bimetallic Catalysts: Discoveries, Concepts, and Applications* (Wiley, New York, 1983).
[18] L. Zhu, R. P. Wang, S. K. Terry, and A. E. DePristo, J. Catal. **167**, 408 (1997).
[19] N. Toshima and T. Yonezawa, New J. Chem. **22**, 1179 (1998).
[20] F. Baletto and R. Ferrando, Rev. Mod. Phys. **77**, 371 (2005).
[21] N. Toshima, M. Harada, T. Yonezawa, K. Kushihashi, and K. Asakura, J. Phys. Chem. **95**, 7448 (1991).
[22] N. Toshima, M. Harada, Y. Yamazaki, and K. Asakura, J. Phys. Chem. **96**, 9927 (1992).
[23] R. Harpeness and A. Gedanken, Langmuir **20**, 3431 (2004).
[24] N. Toshima, M. Kanemaru, Y. Shiraishi, and Y. Koga, J. Phys. Chem. B **109**, 16326 (2005).
[25] J. M. Montejano-Carrizales, M. P. Iñiguez, and J. A. Alonso, Phys. Rev. B **49**, 16649 (1994).
[26] E. B. Krissinel and J. Jellinek, Chem. Phys. Lett. **272**, 301 (1997).
[27] F. Baletto, C. Mottet, and R. Ferrando, Phys. Rev. B **66**, 155420 (2002).
[28] F. Baletto, C. Mottet, and R. Ferrando, Eur. Phys. J. D **24**, 233 (2003).
[29] F. Baletto, C. Mottet, A. Rapallo, and G. Rossi, Surf. Sci. **566-568**, 192 (2004).
[30] J. Guevara, A. M. Llois, F. Aguilera-Granja, and J. M. Montejano-Carrizales, Physica B **354**, 300 (2004).
[31] L. D. Lloyd, R. L. Johnston, S. Salhi, and N. T. Wilson, J. Mater. Chem. **14**, 1691 (2004).
[32] G. Rossi, A. Rapallo, C. Mottet, A. Fortunell, F. Baletto, and R. Ferrando, Phys. Rev. Lett. **93**, 105503 (2004).
[33] G. F. Wang, M. A. VanHove, P. N. Ross, and M. I. Baskes, J. Chem. Phys. **121**, 5410 (2004).
[34] A. Rapallo, G. Rossi, R. Ferrando, A. Fortunelli, B. C. Curley, L. D. Lloyd, G. M. Tarbuck, and R. L. Johnson, J. Chem. Phys. **122**, 194308 (2005).
[35] G. F. Wang, M. A. VanHove, P. N. Ross, and M. I. Baskes, Prog. Surf. Sci. **79**, 28 (2005).
[36] G. F. Wang, M. A. VanHove, P. N. Ross, and M. I. Baskes, J. Phys. Chem. B **109**, 11683 (2005).
[37] A. Mañanes, M. P. Iñiguez, M. J. López, and J. A. Alonso, Phys. Rev. B **42**, 5000 (1990).
[38] C. Massen, T. V. Mortimer-Jones, and R. L. Johnston, J. Chem. Soc. Dalton Trans. **23**, 4375 (2002).

[39] F. Baletto, C. Mottet, and R. Ferrando, Phys. Rev. Lett. **90**, 135504 (2003).
[40] M. M. Mariscal, S. A. Dassie, and E. P. M. Leiva, J. Chem. Phys. **123**, 184505 (2005).
[41] G. F. Wang, M. A. VanHove, P. N. Ross, and M. I. Baskes, J. Chem. Phys. **122**, 024706 (2005).
[42] C. Mottet, G. Rossi, F. Baletto, and R. Ferrando, Phys. Rev. Lett. **95**, 035501 (2005).
[43] B. J. Hwang, L. S. Sarma, J. M. Chen, C. H. Chen, S. C. Shih, G. R. Wang, D. G. Liu, J. F. Lee, and M. T. Tang, J. Am. Chem. Soc. **127**, 11140 (2005).
[44] J. L. Wang, F. Ding, W. F. Shen, and T. X. Li, Solid State Commun. **119**, 13 (2001).
[45] Y. G. Chushak and L. S. Bartell, J. Phys. Chem. B **107**, 3747 (2003).
[46] S. P. Huang and P. B. Balbuena, J. Phys. Chem. B **106**, 7225 (2002).
[47] S. K. R. S. Sankaranarayanan, V. R. Bhethanabotla, and B. Joseph, Phys. Rev. B **71**, 195415 (2005).
[48] S. K. R. S. Sankaranarayanan, V. R. Bhethanabotla, and B. Joseph, Phys. Rev. B **72**, 195405 (2005).
[49] K. Joshi and D. G. Kanhere, Phys. Rev. A **65**, 043203 (2002).
[50] K. Joshi and D. G. Kanhere, J. Chem. Phys. **119**, 12301 (2003).
[51] A. Aguado, L. E. González, and M. J. López, J. Phys. Chem. B **108**, 11722 (2004).
[52] A. Aguado, M. J. López, and S. Núñez, Comput. Mater. Sci. **35**, 174 (2006).
[53] A. Aguado and J. M. López, Phys. Rev. B **72**, 205420 (2005).
[54] A. Aguado and J. M. López, Phys. Rev. B **71**, 075415 (2005).
[55] T. Van Hoof and M. Hou, Phys. Rev. B **72**, 115434 (2005).
[56] F. Cleri and V. Rosato, Phys. Rev. B **48**, 22 (1993).
[57] L. Gomez, A. Dobry, and H. T. Diep, Phys. Rev. B **55**, 6265 (1997).
[58] F. Ding, A. Rosen, and K. Bolton, Phys. Rev. B **70**, 075416 (2004).
[59] E. G. Noya, J. P. K. Doye, and F. Calvo, Phys. Rev. B **73**, 125407 (2006).
[60] J. Westergren and S. Nordholm, Chem. Phys. Lett. **290**, 189 (2003).
[61] J. Westergren, S. Nordholm, and A. Rosén, Phys. Chem. Chem. Phys. **5**, 136 (2003).
[62] X. J. Han, M. Chen, and Z. Y. Guo, J. Phys.: Condens. Matter **16**, 705 (2004).
[63] H. Reichert and H. Dosch, Surf. Sci. **345**, 27 (1996).
[64] A. Maidou and H. M. Polatoglou, Phys. Rev. B **60**, 9145 (1999).
[65] M.-J. Kim, H.-J. Na, K. C. Lee, E. A. Yoo, and M. Y. Lee, J. Mater. Chem. **13**, 1789 (2003).
[66] M. J. López, P. A. Marcos, and J. A. Alonso, J. Chem. Phys. **104**, 1056 (1996).
[67] T. Van Hoof and M. Hou, Appl. Surf. Sci. **226**, 94 (2004).
[68] N. T. Wilson and R. L. Johnson, J. Mater. Chem. **12**, 2913 (2002).
[69] S. Darby, T. V. Mortimer-Jones, R. L. Johnson, and C. Roberts, J. Chem. Phys. **116**, 1536 (2002).
[70] D. Cheng, S. Huang, and W. Wang, Eur. Phys. J. D **39**, 41 (2006).
[71] S. M. Foiles, Phys. Rev. B **32**, 7685 (1985).
[72] *Surface Segregation Phenomena*, edited by S. M. Foiles, P. A. Dowben, and A. Miller (CRC Press, Boca Raton, 1990).
[73] E. E. Zhurkin and M. Hou, J. Phys.: Condens. Matter **12**, 6735 (2000).
[74] T. X. Li, Y. L. Ji, S. W. Yu, and G. H. Wang, Solid State Commun. **116**, 547 (2000).
[75] J. M. Soler, M. R. Beltran, K. Michaelian, I. L. Garzon, P. Ordejon, D. Sanchez-Portal, and E. Artacho, Phys. Rev. B **61**, 5771 (2000).